DESIGN OF OPTIMAL OBSERVATION STRATEGY FOR RE-ENTRY PREDICTION IMPROVEMENT OF GTOS UPPER STAGE

G. Di Mauro[(1)], M. Rasotto[(1)], M. Massari[(2)], P. Di Lizia[(2)], R. Armellin[(3)], Q. Funke[(4)] and T. Flohrer[(5)]

[(1)] Dinamica SrL, Italy
[(2)] Politecnico di Milano, Department of Aerospace Science and Technology, Italy
[(3)] University of Southampton, Faculty of Engineering and the Environment, UK
[(4)] IMS SPACE CONSULTANCY GMBH c/o ESA-ESOC, Germany
[(5)] ESA-ESOC, Germany

ABSTRACT

In this paper, an automatic approach to design the observation strategy of spent upper stage moving on GTOs is presented. More specifically, the design is formulated as a multi-objective optimization problem solved by means of a multi-objective genetic algorithm (MOGA). This approach allows minimizing both the number of total measurements required to detect the object and the error on re-entry prediction. Within the optimization process a nonlinear OD algorithm is run to determine the estimates of both initial state and model parameters and the associated covariance matrix. The Nonlinear Least Square Estimator (NLSE) technique is implemented, exploiting the differential algebra framework for Jacobian matrix computation in order to reduce the computational effort related to OD problem solution. Finally, the software tool IRIS is developed to accurately simulate the observation campaign based on geometry and constraints of existing sensors currently available to the European Space Agency (ESA). Numerical simulations are performed to demonstrate the efficiency of the proposed approach.

Index Terms— Observation simulator, observation strategy design

1 INTRODUCTION

From 2004 up to the date more than 200 launch vehicles operated by five independent nations and two international organizations placed satellites in Geostationary Earth Orbit (GEO). In almost all cases, each successful launch left one or more pieces of debris in Geostationary Transfer Orbits (GTO). Particularly, many of this space debris consist of large spent upper stages of launch vehicles whose atmosphere re-entry might violate the constraint on casualty risk of 1/10000: as of 16 October 2014, it is expected that about 79 spent upper stages operating on GTOs with an inclination lower than 20 degree will enter the Earth atmosphere in the next 200 years. Moreover, the GTOs are highly eccentric orbits with perigee normally at low altitudes (170–650 km) and the apogee near geo-stationary altitude (35,780 km). Thus, space debris in GTOs generally passes through densely populated regions such as Low Earth Orbit (LEO) and GEO regions, being a hazard for the safety of other operating spacecraft. In light of the above, the improvement of re-entry prediction of GTO spent upper stages is a key issue to manage both on-orbit collision risk and on-ground casualty risk.

Currently the only public data source available for re-entry prediction of a space object are represented by Two Line Elements (TLEs), provided by the United States Strategic Command (USSTRATCOM). However, this set of data are inaccurate and do not come with uncertainty information, making their use in re-entry prediction challenging, especially for the GTO space objects. This leads to the need of using the observational data to improve the re-entry prediction.

The design of observation strategy for GTO upper stage is not trivial. The detection and tracking of space objects on GTOs might require more than a single sensor in fact, since the distance from the observer has large variation along the orbit; this multiple sensors configuration might involve problems such as scheduling or data fusion, making the observation complex and costly. In addition, design of an optimal observation strategy for improvement of re-entry prediction involves the definition of a high-accuracy orbit determination (OD) algorithm, and the implementation of proper methods for uncertainty mapping. This might require the definition of accurate dynamical models in order to describe the effects of third-body perturbations and the Earth's oblateness and to capture the intricacies of re-entry phase, as well as the use of nonlinear technique for orbit determination.

An approach to design the observation strategy is here presented. It tackles the detection strategy design problem as a multi-objective optimization problem and solves it using a genetic algorithm.

The rest of the paper is organized as follows. In section 2 the software tool developed for the simulation of observation campaigns is presented; in section 3 the orbit determination problem is addressed and the Nonlinear Least

Square Estimator (NLSE) algorithm is briefly summarized; section 4 details the proposed approach for the observation strategy design; finally section 5 shows the results regarding the observation strategy designed for some studied cases.

2 OBSERVATION SIMULATOR

The design of the optimal observation strategy requires an accurate analysis of space object dynamics as well as the characterization of the sensors used for observing. For this reason we developed the software tool IRIS, which accurately simulates the space object motion and its detection through a specific sensor network.

The developed tool is based on the automatic generation of SPICE[1] kernels for both space object trajectories and observatories: once the user has set the initial space object state and the model parameters, such as the object area-to-mass ratio, the tool computes the object trajectory through a high-fidelity orbital propagator, referred to as AIDA, and generates its corresponding kernel through SPICE functions; similarly, it generates the kernels for the defined list of observatories, once the user has set the geodetic coordinates for the sensors. Once object and observatories kernels are built, IRIS uses all powerful features of SPICE to define the relative geometry between space object and observer/s. Finally, depending on the user-defined features of the sensor, the tool is capable to determine the visibility constraints and, then, compute the visibility windows, the observables, and the measures (see Fig. 1).
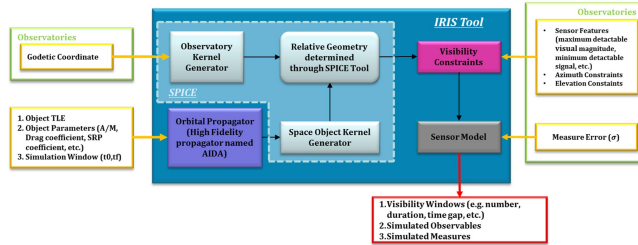

Fig. 1. IRIS tool architecture

It is worth pointing out that a simplified model for the sensor is considered in IRIS. More specifically, all measurement errors due to line transmission, optic geometry, and so on, are described by a normal distribution with mean zero and a standard deviation equal to σ, i.e.,

$$Meas.^{True} = Meas.^{Simulated} + \aleph(0; \sigma). \qquad (1)$$

2.1 Visibility Constraints

The possibility to detect an object orbiting the Earth depends on its orbital configuration, on the geographical position of the observatory, and on sensor capability. All

---

[1] https://naif.jpl.nasa.gov/naif/index.html

these constraints are implemented in IRIS tool and their mathematical formulation is described in what follows.

2.1.1 Geometrical Constraints

Regardless the type of observatory, the object has to be detectable from sensor location. This means that azimuth, β^{Obj}, and elevation, el^{Obj}, of the space object shall be included in the admissible range of the observatory, i.e.

$$\beta_{MIN}^{Obs} < \beta^{Obj} < \beta_{MAX}^{Obs}$$
$$el_{MIN}^{Obs} < el^{Obj} < el_{MAX}^{Obs} \qquad (2)$$

2.1.2 Optical Sensor Constraints

When an optical sensor is used to observe the object, the illumination conditions are crucial. More specifically, to get a measurement from a telescope
(a) the object must be illuminated by the Sun,
(b) its brightness must exceed that of the background sky by a certain margin,
(c) the Sun elevation must be lower than a reference value, i.e. the observation must occur during the night,
(d) the sky must be clear enough, and
(e) the object velocity doesn't exceed a reference value.
If the case of a cylindrical Earth shadow is considered, the first statement (a) turns out in following condition:

$$\phi > \bar{\phi}$$
$$\phi = cos^{-1}\left(\frac{r_{Eart}^{Obj} \cdot r_{Sun}^{Earth}}{\|r_{Earth}^{Obj} \cdot r_{Sun}^{Eart}\|}\right) \qquad (3)$$
$$\bar{\phi} = sin^{-1}\left(\frac{r_E}{\|r_{Earth}^{Obj}\|}\right)$$

where r_{Earth}^{Obj} and r_{Sun}^{Earth} are the position vector between the object and the Earth and between the Earth and the Sun respectively, whereas r_E indicates the terrestrial radius.
For what concerns the object brightness, V^{Obj}, it must be lower than the maximum detectable apparent magnitude of the sensor, $\bar{V}(\beta^{Obj}, el^{Obj}, t_{exposure})$, i.e. $V^{Obj} < \bar{V}$. The object brightness can be computed as, [1]

$$V^{Obj} = -26.78 - 2.5log\left(\frac{A * \varepsilon * F(\varphi)}{(r_{Obs}^{Obj})^2}\right) + \qquad (4)$$
$$+ \frac{0.04}{cos(\pi/2 - el^{Obj})}$$

where A is the sphere's cross-sectional area, ε is the satellite's albedo, -26.78 is the value of apparent visual magnitude of the Sun, and $F(\varphi)$ is a function of phase angle, φ. The phase angle is defined as the angle between

the direction of the observer and the direction of the Sun as seen from the space object. Under the hypothesis of a spherical object, the phase function can be computed as, [2] and [3],

$$F(\varphi) = \frac{2}{3\pi^2} [(\pi - \varphi)\cos(\varphi) + \sin(\varphi)] \qquad (5)$$

Note that the last term in Eq.(5) is added to take into account the attenuation due to the atmosphere absorption; it is singular for $el^{Obj} = 0$, but Eq. (5) is still valid since objects with elevation below 5 deg are excluded from observations. Moreover, without loss of generality, the maximum detectable apparent magnitude of the optical sensor is assumed to be constant; in other word its dependency from angular velocity and exposure time is ignored.

In addition, to guarantee a dark background during observations, the Moon has to be "far enough" from the space object; this turns out in a constraint on angle, γ_{MOON}, between the object-observer vector, $\boldsymbol{r}_{Obs}^{Obj}$, and Moon-observer vector $\boldsymbol{r}_{Obs}^{Moon}$, that is

$$\gamma_{MOON} > \bar{\gamma}_{MOON} = 30 \, deg \qquad (6)$$

Finally, the optical sensor should be in darkness while observing the space object; the necessary degree of darkness depends on the apparent magnitude of the space object. However, in IRIS we set the nautical twilight as the required darkness degree, i.e. $el^{SUN} < -12 \, deg$, [3].

In addition to the aforementioned constraints other conditions should occur to allow using an optical sensor for space object observation. Firstly, the sky has to be clear of clouds. To implement this constraint in IRIS, all measurements that do not satisfy the condition

$$U(0,1) < CCP/100 \qquad (7)$$

are discarded. In Eq. (7) $U(0,1)$ represents a random sample $\in [0,1]$ generated from a uniform distribution, whereas CCP (Cloud Coverage Percentage) indicates the percentage of nights clear of clouds. Another key aspect in optical measuring is the object velocity relative to the observatory. In fact, the object should move slowly enough to guarantee that tracklet is included in sensor FOV within exposure time.

As illustrated in Fig. 2 different situations can occur when the sensor shutter is open: the optical sensor can provide a measurement only if cases B, D, or F occur. However, in IRIS tool we assume that only case F is admissible; in other words, we assume that only the object entirely included in sensor FOV are detectable, such that IRIS gives an optical measurements only when the following conditions come about:

$$\dot{\beta}^{Obj} < \frac{FOV}{Time\ of\ Exposure}$$
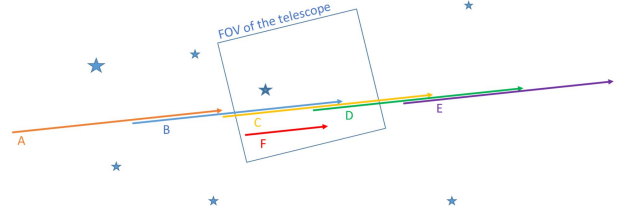$$\dot{el}^{Obj} < \frac{FOV}{Time\ of\ Exposure} \qquad (8)$$

Fig. 2. Possible positions of the tracklet at the shutter actuation time

2.1.3 Radar Sensor Constraints

The detectability of an object by means of radar observation depends on the radar power budget. Thus, it is important to determine the Signal-to-Noise Ratio (SNR) at the receiver to determine whether or not an object can be observed. More specifically, the received power has to be higher than the minimum detectable signal (MDS), i.e.

$$P_r > MDS$$

$$P_r = \frac{P_t * G_{TX} * G_{RX} * \lambda^2 * RCS * L_{TX} * L_{RX}}{(4\pi)^3 (r^{Obj}{}_{RX} * r^{Obj}{}_{TX})^2} \qquad (9)$$

$$MDS = \frac{P_t * G_{TX} * G_{RX} * \lambda^2 * \overline{RCS} * L_{TX} * L_{RX}}{(4\pi)^3 (\overline{r_{RAD}})^4}$$

In Eq. (9) P_t is the transmitter power, G_{RX}/G_{RX} is the receiver/transmitter gain, L_{RX}/L_{TX} is the loss due to atmosphere disturbance in receiver/transmitter track, λ is the wavelength, and RCS indicate the radar cross-section. $\overline{RCS}$ and $\overline{r_{RAD}}$ are reference values for radar cross-section and distance between object and observer respectively, which depends on observatory capability.

3 ORBIT DETERMINATION

The objective of orbit determination (OD) is to obtain an accurate orbit that accounts for the dynamical environment in which the motion occurs, including all relevant forces affecting the satellite's motion, given a large set of tracking data. In other words, the goal of OD is to determine initial condition for the position and velocity, $\boldsymbol{x}_0 = [\boldsymbol{r}_0 \quad \boldsymbol{v}_0]^T \in \mathfrak{R}^n$, as well as for model parameters, $\boldsymbol{p} \in \mathfrak{R}^s$, from the sensor measurements.

The general procedure for OD algorithms is to set up a dynamical model of the orbit that uses observations to improve the parameters of the orbit by the process of differential corrections, [4]. Since dynamics and measurement models are generally nonlinear, the OD

problem solution might be tough: the linear assumption can sometimes fail to characterize the true spacecraft dynamics and statistics when a system is subject to a highly unstable environment or when mapped over a long duration of time.

In light of the above, in this study we considered nonlinear approach for the OD of GTOs objects. Particularly, we investigated the Nonlinear Least Squares Estimator (NLSE). The advantage of this method is that any type of measurement can be processed; moreover, it provides the uncertainty of the estimated states. In what follows a brief description of NLSE is given.

3.1 Nonlinear Least Squares Estimator (NLSE)

The basic idea of least-squares estimation as applied to OD problem is to find the trajectory and model parameters for which the square of the difference between the modelled observations and the actual measurements becomes as small as possible, [5]. In order to derive the mathematical formulation of NLSE, let

$$\boldsymbol{\xi} = [\boldsymbol{x}(t) \quad \boldsymbol{p}]^T \tag{10}$$

denote a $(n + s)$-dimensional vector comprising the object state vector (position and velocity vector, i.e. $\boldsymbol{x}(t) = [\boldsymbol{r} \quad \boldsymbol{v}]^T$) and the parameters $\boldsymbol{p} \in \Re^s$ that affect the force and measurement models. The time evolution of $\boldsymbol{x}$ can be described by an ordinary differential equation of the form,

$$\dot{\boldsymbol{x}}(t) = \boldsymbol{f}(t; \boldsymbol{\xi})$$
$$\boldsymbol{x}_0 = \boldsymbol{x}(t_0) \tag{11}$$

where $\boldsymbol{f}(t; \boldsymbol{\xi})$ represents the system dynamics vector with a dimension n. Furthermore, let

$$\boldsymbol{z} = [z_1 \quad \dots \quad z_m]^T \tag{12}$$

denote a m-dimensional vector of measurements taken at times $t_1, \dots, t_m$. The observations can be described by the following model, [5]:

$$\boldsymbol{z} = \boldsymbol{g}(t; \boldsymbol{\xi}) + \boldsymbol{v} = \boldsymbol{h}(t; \boldsymbol{x}_0, \boldsymbol{p}) + \boldsymbol{v} \tag{13}$$

where $\boldsymbol{g}(t; \boldsymbol{\xi})$ represents the measurements function, whereas vector $\boldsymbol{v}$ accounts for measurement errors that occur at each observation, assumed to be randomly distributed with zero-mean value. Defining the residual error associated with the measurement vector as

$$\boldsymbol{e} = \boldsymbol{z} - \hat{\boldsymbol{z}} = \boldsymbol{z} - \boldsymbol{h}(t; \hat{\boldsymbol{x}}_0, \hat{\boldsymbol{p}}) \tag{14}$$

the least-squares OD problem is defined as finding the $\hat{\boldsymbol{x}}_0$ and $\hat{\boldsymbol{p}}$ that minimize the loss function

$$J = \frac{1}{2} \boldsymbol{e}^T \boldsymbol{e} = \left(\boldsymbol{z} - \boldsymbol{h}(t; \hat{\boldsymbol{x}}_0, \hat{\boldsymbol{p}}) \right)^T \boldsymbol{W} \left(\boldsymbol{z} - \boldsymbol{h}(t; \hat{\boldsymbol{x}}_0, \hat{\boldsymbol{p}}) \right), \tag{15}$$

where $\boldsymbol{W}$ is a $m \times m$ diagonal matrix in which the elements w_k are set as the reciprocal of the measurement error variances.

Since $\boldsymbol{h}(t; \hat{\boldsymbol{x}}_0, \hat{\boldsymbol{p}})$ is a highly non-linear function of the unknown $\hat{\boldsymbol{x}}_0$ and $\hat{\boldsymbol{p}}$, the minimization of function J might be difficult. Thus, the NLSE requires, firstly, the linearization of $\boldsymbol{h}(t; \hat{\boldsymbol{x}}_0, \hat{\boldsymbol{p}})$ around a reference state, $\hat{\boldsymbol{x}}_{ref}$, and a reference parameter vector, $\boldsymbol{p}_{ref}$, that is

$$\boldsymbol{h}(t; \hat{\boldsymbol{x}}_0, \hat{\boldsymbol{p}}) = \boldsymbol{h}(t; \hat{\boldsymbol{x}}_{0,ref}, \hat{\boldsymbol{p}}_{ref}) + \frac{\partial \boldsymbol{h}}{\partial \boldsymbol{x}_0}(\hat{\boldsymbol{x}}_0 - \hat{\boldsymbol{x}}_{0,ref})$$
$$+ \frac{\partial \boldsymbol{h}}{\partial \boldsymbol{p}}(\hat{\boldsymbol{p}} - \hat{\boldsymbol{p}}_{ref}) = \tag{16}$$
$$= \boldsymbol{h}(t; \hat{\boldsymbol{x}}_{0,ref}, \hat{\boldsymbol{p}}_{ref}) + \boldsymbol{H} \begin{bmatrix} \Delta \hat{\boldsymbol{x}} \\ \Delta \hat{\boldsymbol{p}} \end{bmatrix}$$

where

$$\boldsymbol{H} = \begin{bmatrix} \dfrac{\partial \boldsymbol{h}}{\partial \boldsymbol{x}_0} & \dfrac{\partial \boldsymbol{h}}{\partial \boldsymbol{p}} \end{bmatrix} = \begin{bmatrix} \dfrac{\partial \boldsymbol{g}}{\partial \boldsymbol{x}} \dfrac{\partial \boldsymbol{x}}{\partial \boldsymbol{x}_0} & \dfrac{\partial \boldsymbol{g}}{\partial \boldsymbol{x}} \dfrac{\partial \boldsymbol{x}}{\partial \boldsymbol{p}} \end{bmatrix} = [\boldsymbol{H}_1 \quad \boldsymbol{H}_2] \tag{17}$$

and

$$\Delta \hat{\boldsymbol{x}} = (\hat{\boldsymbol{x}}_0 - \hat{\boldsymbol{x}}_{0,ref})$$
$$\Delta \hat{\boldsymbol{p}} = (\hat{\boldsymbol{p}} - \hat{\boldsymbol{p}}_{ref}) \tag{18}$$

The OD problem can be reduced to find $\Delta \hat{\boldsymbol{x}}$ and $\Delta \hat{\boldsymbol{p}}$ such that the loss function,

$$J = \frac{1}{2} \left(\Delta \boldsymbol{z} - \boldsymbol{H} \begin{bmatrix} \Delta \hat{\boldsymbol{x}} \\ \Delta \hat{\boldsymbol{p}} \end{bmatrix} \right)^T \boldsymbol{W} \left(\Delta \boldsymbol{z} - \boldsymbol{H} \begin{bmatrix} \Delta \hat{\boldsymbol{x}} \\ \Delta \hat{\boldsymbol{p}} \end{bmatrix} \right),$$
$$\Delta \boldsymbol{z} = \boldsymbol{z} - \boldsymbol{h}(t; \hat{\boldsymbol{x}}_{0,ref}, \hat{\boldsymbol{p}}_{ref}) \tag{19}$$

is minimum, that is

$$\frac{\partial J}{\partial (\Delta \hat{\boldsymbol{\xi}}_0^T)} = \frac{\partial J}{\partial ([\Delta \hat{\boldsymbol{x}} \quad \Delta \hat{\boldsymbol{p}}])} = \boldsymbol{0}. \tag{20}$$

If the Jacobian matrix $\boldsymbol{H}$ has full rank, the minimization of J leads to the following solution,

$$\begin{bmatrix} \Delta \hat{\boldsymbol{x}} \\ \Delta \hat{\boldsymbol{p}} \end{bmatrix} = (\boldsymbol{H}^T \boldsymbol{W} \boldsymbol{H})^{-1} \boldsymbol{H}^T \boldsymbol{W} \Delta \boldsymbol{z} \tag{21}$$

Since the nonlinearity of $\boldsymbol{h}$, the simplified loss function in Eq. (19) differs slightly from the rigourous one and the estimates $\hat{\boldsymbol{x}}_0 = \hat{\boldsymbol{x}}_{0,ref} + \Delta \hat{\boldsymbol{x}}$ and $\hat{\boldsymbol{p}} = \hat{\boldsymbol{p}}_{ref} + \Delta \hat{\boldsymbol{p}}$ don't represent the exact solution of OD problem. In order to improve the OD solution, the NLSE algorithm provides a successive approximation procedure that converges to accurate least squares estimates, given approximate starting values, $\hat{\boldsymbol{x}}_0^0$ and $\hat{\boldsymbol{p}}^0$. More specifically, the non-linear problem can be solved by following iteration, [6],

$$\Delta \boldsymbol{z}^j = \boldsymbol{z} - \boldsymbol{h}(t; \hat{\boldsymbol{x}}_0^j, \hat{\boldsymbol{p}}^j) \tag{22}$$

$$\Delta \xi^j = \begin{bmatrix} \Delta \hat{x} \\ \Delta \hat{p} \end{bmatrix}^j = (H^{j,T} W H^j)^{-1} H^{j,T} W \Delta z^j$$

$$\hat{x}_0^{j+1} = \hat{x}_0^j + \Delta \hat{x}^j$$

$$\hat{p}^{j+1} = \hat{p}^j + \Delta \hat{p}^j$$

started from $\hat{x}_0^0 = \hat{x}_{0,ref}$ and $\hat{p}^0 = \hat{p}_{ref}$ and continued until the relative change of the loss function J is smaller than a prescribed tolerance for successive approximations, that is

$$\delta J = \frac{|J_j - J_{j-1}|}{J_j} < \frac{\varepsilon}{\|W\|} \tag{23}$$

$$J_j = \Delta z^{j,T} W \Delta z^j$$

Then, the NLSE can be summarized as follow:

1. Initialize the estimates $\hat{x}_0^0$ and $\hat{p}^0$ as $\hat{x}_0^0 = \hat{x}_{0,ref}$ and $\hat{p}^0 = \hat{p}_{ref}$ respectively;
2. Compute Δz^j and $\Delta \xi^j$ as illustrated in Eqs. (22);
3. Evaluate the stop criterion δJ reported in Eq. (23);
4. Update the estimate (see the last in Eqs. (22))
5. Repeat steps 2 and 4 until $\delta J < \varepsilon/\|W\|$ or the number of iterations is smaller than the maximum allowable number of iterations, N_{iter}^{max}.

It is worth mentioning that we use the differential algebra (DA) framework to compute the Jacobian matrix H, [7]; this approach allows reducing the time required for computation of Jacobian matrix with respect to the standard approach based on finite differences. It is worth mentioning that DA is implemented in a computer environment through a software tool, named Differential Algebra Computer Engine (DACE), developed by DINAMICA in 2014, [8].

4   OBSERVATION STRATEGY DESIGN

The design of an optimal observation strategy is not a trivial task, even when the sensor architecture is given, i.e. the type/features of available sensors as well as their locations are known. Even in this case, in fact, the choice of the "best" strategy depends on the orbital configuration of the studied object and on the epoch in which the campaign starts, that affects the illumination conditions as well as the relative position between the observer and the object.

This section presents the proposed approach to determine the optimal observation strategy when specific sensor architecture is used.

4.1   Optimization Approach

The proposed approach tackles the detection strategy design problem as a multi-objective optimization problem (MOOP). More specifically, the method proposed in this study is based on the use of a multi-objective evolutionary algorithm, such as *multi-objective genetic algorithm* (MOGA). In fact, since evolutionary algorithms deal simultaneously with a set of possible solutions (the so-called

population), they allows finding an entire set of Pareto optimal solutions in a single run of the algorithm, instead of having to perform a series of separate runs as in the case of the traditional mathematical programming techniques. Additionally, they are less susceptible to the shape or continuity of the Pareto front, whereas these two issues are a real concern for mathematical programming techniques, [9]. The optimization approach for the strategy design consists of the following steps:

1. *Generate Pseudo-observations*. For a given object to be studied, one has to generate an accurate trajectory between the initial epoch, t_0, and the final one, t_f, and then simulates the observation campaign through IRIS tool (see section 2).
2. *Run MOGA*. A MOGA is run in order to minimize the number of measurements and the maximum uncertainty on the estimated state/parameters given by OD algorithm. In light of the above, the objective function is given by the following 2-dimensional vector,

$$f(X_{opt}) = \begin{Bmatrix} f_1(X_{opt}) \\ f_2(X_{opt}) \end{Bmatrix} = \begin{Bmatrix} N_{Obs} \\ max(\lambda_i) \end{Bmatrix}, \tag{24}$$

where N_{Obs} is the number of observations, λ_i is *i-th* eigenvalue of the covariance matrix of the OD solution. X_{opt} is the optimization vector, defined as a bit-string vector: since the aim is to find the optimal measurements combination, each individual in MOGA is in fact represented by a bit (0 or 1), where 1 indicates that the corresponding observation is hold whereas 0 indicates that the corresponding observation is discarded. Therefore, X_{opt} has the form $X_{opt} = [1,0,0,1,\ldots,0,0,1] \in \Re^{N_{Obs}}$. At each MOGA iteration the NLSE is used to compute the estimates of initial state/parameters as well as the associated covariance matrix (see section 3.1). The MOGA iterates until a Pareto front is computed.
3. *Select a solution on the Pareto-front*. The MOGA provides a Pareto front of optimal solutions. Among them, a solution can be chosen using the following relation:

$$f_{opt} = \alpha f_1 + (1 - \alpha) f_2 \tag{25}$$

where α is a constant value assumed to be equal to 0.5; this guarantees that both objective functions have the same weight.

It is worth remarking that the definition of the optimal observation strategy is based on the performance of the OD rather than on the evaluation of the error between the predicted state and the real one at the re-entry epoch, besides on the number of observations. The real trajectory is not known in fact. In light of this, at step 2 a spectral

decomposition of covariance matrix is performed and the largest eigenvalue is minimized. This means that MOGA aims at minimizing the maximum uncertainty value corresponding to $[\widehat{x}_0, \widehat{p}]$. However let us note that this choice doesn't give any insight on how the uncertainty on each component of $[\widehat{x}_0, \widehat{p}]$ affects the re-entry prediction; in fact, the minimization of a specific eigenvalue of covariance matrix might have a greater impact on the re-entry prediction. For the sake of the example, let us consider that OD goal is to estimate only the initial position, $\widehat{r}_0 \in \mathfrak{R}^3$. In this case the uncertainty on the estimated initial position can be represented by a 3-dimensional ellipsoid, as illustrated in Fig. 3. Clearly, each eigenvalue might have a different impact on the error at re-entry epoch. Since the nominal trajectory is not available, the assessment of the most significant direction is not easy to determine; for this reason our approach relies on the selection of the maximum eigenvalue as an index of OD performance, represented in figure by λ_1.
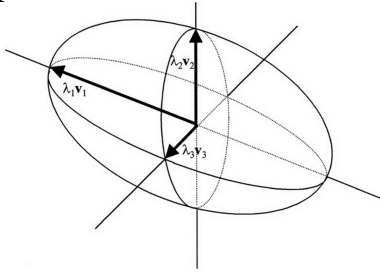

Fig. 3. Example of spectral decomposition of the covariance matrix in 3 dimensions

5   RESULTS

In this study we focus on the GTO spent upper stages for the design of optimal observation strategy. In particular, we consider five upper stages, each representing a specific class identified according to the initial orbital configuration, i.e. to i_0 and ω_0 (see Fig. 4). Table. 1 reports the initial inclination and argument of perigee of all selected objects.

Table. 1. Orbital configuration and A/M for five selected objects

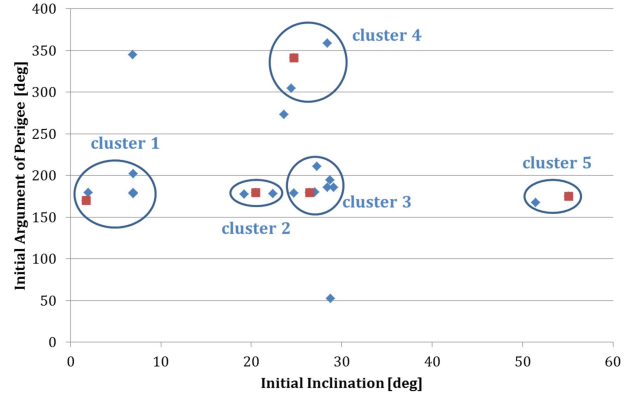| Norad ID	Name	Nominal A/M (m^2/kg)	i_0 (deg)	ω_0 (deg)
37239	Ariane 5 second stage	0.008423	1.77	169.86
37211	CZ-3C third stage	0.011697	20.48	179.45
21990	Atlas IIA second stage	0.012189	26.45	179.06
07794	Delta 2914 third stage	0.01061	24.75	340.62
37949	CZ-3A third stage	0.011697	55.12	174.84

Fig. 4. Initial inclination and argument of perigee for 25 GTO objects; the red dots represent the 5 objects representative of object clusters

In what follows the results obtained through the optimization approach are illustrated. For the sake of brevity only the results concerning the second state of Ariane (37239) launcher and the third stage of CZ-3A launcher (37949) are shown. In addition we assume that the measurements are provided by the sensor network consisting of following five observatories:

- *Teide Observatory* (referred to as OGS from now on), Tenerife (Canary Islands/Spain);
- *Zimmerwald observatory* (referred to as ZIMLAT from now on), Bern (Switzerland);
- *Tracking & Imaging Radar* (TIRA), Bonn (Germany)
- *Monopulse Surveillance Secondary Radar* (MSSR);
- *Bistatic Surveillance Secondary Radar* (BSSR).

The NLSE algorithm (see section 3.1) is run at each MOGA iteration assuming an initial random error on position and velocity with a standard deviation of 1 km and 1 m/s respectively, and a displacement from the nominal A/M value of 5%.

Finally, an observation campaign of 10 days is simulated and IRIS tool is exploited to generate the pseudo-observation.

5.1   Ariane 5 Second Stage (37239)

Figure 4 shows the Pareto front obtained through MOGA. It is straightforward that the higher is the numbers of observations, the lower is the value of $max(\lambda_i)$, i.e. the better is the estimates of orbital state and parameters. From the same figure, the Pareto front solution corresponding to $\alpha = 0.5$ is characterized by 14 measures and a maximum eigenvalue of 1.22e-5. The position of measurements along the orbit corresponding to the same solution is shown in Fig. 6. Let us point out that the radar measurements are almost symmetrically dislocated along the orbit, whereas optical observations are all on the same side of the orbit. In fact this

is the only portion in which optical measures are feasible since the position of the Sun relative to the observed object. Furthermore, radar measurements are interestingly taken at quite large distance from the perigee and close to the maximum available bound for this type of sensors. This fact is due to the high latitude of TIRA and to the low inclination of object orbit.

Finally, it is worth remarking that MSSR and BSSR are never involved into the observation process; they provide a high value of minimum detectable signal, making the observation of GTO object unfeasible.
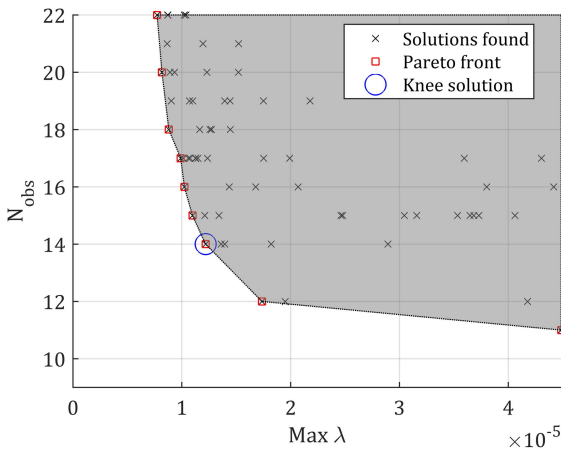

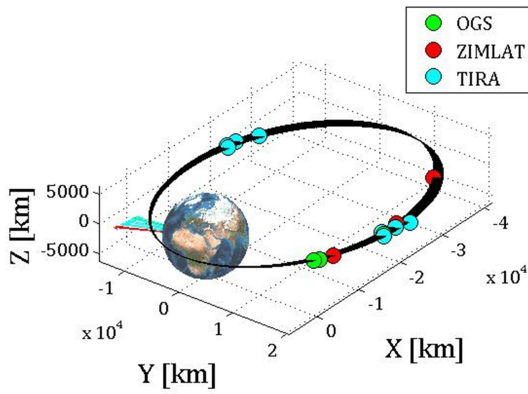**Fig. 5.** Pareto front deriving from optimization approach for object 37239

Fig. 6. Measurements distribution along the orbit corresponding to α=0.5 for object 37239; arrows represent the Sun-Earth vector at measure epochs

5.2   CZ-3A Third Stage (37949)

Figures 7 - 8 illustrate the Pareto-front given by MOGA and the measurements distribution along the orbit corresponding to $\alpha = 0.5$ respectively. The Pareto front knee-solution ($\alpha = 0.5$) is characterized by 16 measures and a maximum eigenvalue of 1.619e-5.

From Fig. 8 the optical instruments, i.e. OGS and ZIMLAT, detect the object when it moves around the orbit apogee, whereas TIRA can observe the object when it is close to orbit perigee. In addition, note that TIRA provides measures only when the object moves on the part of the orbit above the celestial equator. This is mainly due to high inclination of orbit ($i_0 = 55.12°$) combined with the high latitude of TIRA sensor; when the object is under the celestial equator it is too far or out of visibility cone of the instrument to be detected.
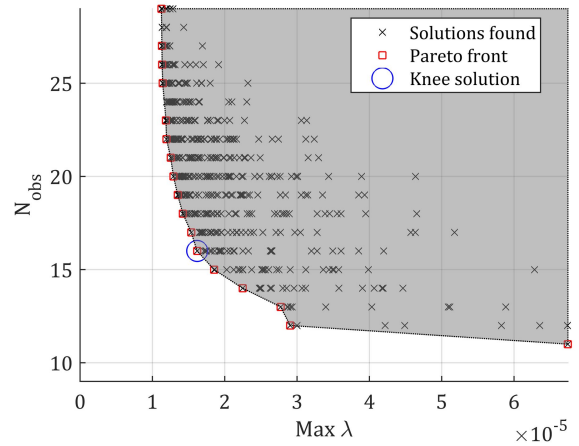

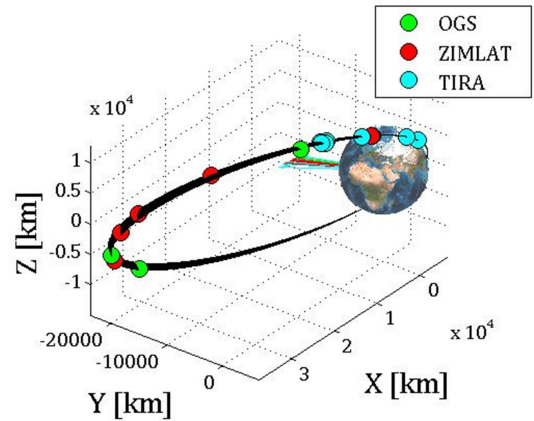**Fig. 7.** Pareto front deriving from optimization approach for object 37949

Fig. 8. Measurements distribution along the orbit corresponding to α=0.5 for object 37949; arrows represent the Sun-Earth vector at measure epochs

6   CONCLUSION

An automatic approach for observation strategy design of spent upper stage in GTO was proposed. It is based on a multi-objective genetic algorithm that aims at minimizing the number of required measures and maximizing the accuracy of deriving orbit determination solution.

Five GTO upper stages are considered to assess the effectiveness of proposed approach. In addition we assumed that the measurements are provided by ESA sensor network, consisting of 2 telescopes and 3 radars. The results show that optimization approach is able to easily generate the optimal observation strategy. Moreover, it allows determining a relation between the number of measurements and the corresponding orbit determination accuracy through the Pareto front. On the other hand, it is very demanding in term of CPU recourse and computational burden.

Finally we developed a high accuracy observation simulator, IRIS, in order to generate the observables for each instrument within the optimization approach.

7 REFERENCES

[1] M. D. Hejduk, "Specular and diffuse components in spherical satellite photometric modelling," Advanced Maui Optical and Space Surveillance Technologies Conference, September 2011.

[2] R. Tousey, "Optical problems of the satellite," Journal of Optical Society of America, vol. 47, issue 4, pp. 261–267, 1957.

[3] G. Veis, "Optical Tracking of Artificial Satellites," Space Science Reviews, vol 2, issue 2, pp. 250–296, 1963.

[4] J.R. Vetter, "Fifth Years of Orbit Determination: Development of Modern Astrodynamics Methods," Johns Hopkins Technical Digest, vol. 27, N° 3, 2007.

[5] O. Montenbruck, E. Gill, "Satellites Orbits. Models, Methods and Applications," Springer, 2005.

[6] J.L. Crassidis, J.L. Jankins, "Optimal Estimation of Dynamic Systems," Chapman & Hall/CRC Press LLC, 2004.

[7] M. Berz, "Modern Map Methods in Particle Beam Physics," Academic Press, 1999.

[8] M. Massari, P. Di Lizia, and M. Rasotto, "Nonlinear Uncertainty Propagation in Astrodynamics: Comparing Taylor Differential Algebra with Monte-Carlo on GPUs," 26th AAS/AIAA Space Flight Mechanics Meeting, 14-18 Feb 2016, Napa, CA (USA).

[9] K. C. Tan, E. F. Khor, and T. H. Lee, "Multiobjective Evolutionary Algorithms and Applications," Springer, 2005.